

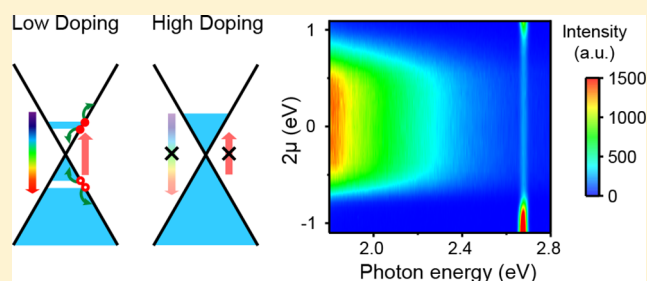
## Gate Switching of Ultrafast Photoluminescence in Graphene

Di Huang,<sup>†</sup> Tao Jiang,<sup>†</sup> Yu Zhang,<sup>†</sup> Yuwei Shan,<sup>†</sup> Xiaodong Fan,<sup>‡,§</sup> Zhihong Zhang,<sup>||</sup> Yunyun Dai,<sup>†</sup> Lei Shi,<sup>†,⊥</sup> Kaihui Liu,<sup>||</sup> Changan Zeng,<sup>‡,§</sup> Jian Zi,<sup>†,⊥</sup> Wei-Tao Liu,<sup>\*,†,⊥</sup> and Shiwei Wu<sup>\*,†,⊥</sup><sup>†</sup>State Key Laboratory of Surface Physics, Key Laboratory of Micro and Nano Photonic Structures (MOE), and Department of Physics, Fudan University, Shanghai 200433, China<sup>‡</sup>International Center for Quantum Design of Functional Materials, Hefei National Laboratory for Physical Sciences at the Microscale, and Synergetic Innovation Center of Quantum Information and Quantum Physics and <sup>§</sup>CAS Key Laboratory of Strongly-Coupled Quantum Matter Physics, and Department of Physics, University of Science and Technology of China, Hefei, Anhui 230026, China<sup>||</sup>State Key Laboratory for Mesoscopic Physics and School of Physics, Peking University, Beijing 100871, China<sup>⊥</sup>Collaborative Innovation Center of Advanced Microstructures, Nanjing 210093, China

## Supporting Information

**ABSTRACT:** The control of optical properties by electric means is the key to optoelectronic applications. For atomically thin two-dimensional (2D) materials, the natural advantage lies in that the carrier doping could be readily controlled through the electric gating effect, possibly affecting the optical properties. Exploiting this advantage, here we report the gate switching of the ultrafast upconverted photoluminescence from monolayer graphene. The luminescence can be completely switched off by the Pauli-blocking of one-photon interband transition in graphene with an on/off ratio exceeding 100, which is remarkable compared to other 2D semiconductors and 3D bulk counterparts. The chemical potential and pump fluence dependences of the luminescence are nicely described by a two-temperature model, including both the hot carrier dynamics and carrier-optical phonon interaction. This gate switchable and background-free photoluminescence can open up new opportunities for graphene-based ultrafast optoelectronic applications.

**KEYWORDS:** Graphene, gate switching, ultrafast photoluminescence, hot carriers, optoelectronics, two-temperature model



Atomically thin two-dimensional (2D) materials have exhibited enormous potential applications in electronics and optoelectronics since the past decade.<sup>1–5</sup> One major impetus is that the doping level of carriers in these materials could be readily controlled through the electrical gating. Many fascinating phenomena and functionalities based on such electrical doping have been observed and realized in 2D materials.<sup>6–13</sup> Photoluminescence is one of the most fundamental optical processes and is directly related to the dynamics of photoexcited carriers. Therefore, it is expected to be highly susceptible to electric gating, as has already been demonstrated in semiconducting transition metal dichalcogenide monolayers.<sup>8,9</sup> Such gate-controlled photoluminescence has revealed rich physics of excitons (a bound state of electron–hole pairs) and their coupling with charge, spin, valley, and layer degrees of freedom.<sup>14,15</sup> However, there have been few similar studies on graphene, because graphene is a semimetallic material with zero bandgap.<sup>7,16</sup> No photoluminescence upon continuous wave (CW) excitations could be observed, unless the graphene is heavily doped to its one-photon Fermi edge resonance.<sup>7</sup>

In contrast to the CW case, a strong, upconverted, ultrafast photoluminescence emerges from undoped graphene upon the

femtosecond laser excitation, as observed by us and other groups.<sup>16–19</sup> In this work, we investigated this ultrafast photoluminescence from ion-gel gated monolayer graphene and showed that it can be completely switched off by electrical gating with an on/off ratio exceeding 100, due to Pauli-blocking of the one-photon interband transition pathway in heavily doped graphene (Figure 1a). We developed a theoretical model to describe the dependence of this photoluminescence to the chemical potential as well as the pump laser fluence, based on a two-temperature distribution of hot carriers and optical phonons.<sup>18,20,21</sup> This first observation of gate-dependent ultrafast photoluminescence in graphene helps us to gain insight into the hot carrier ultrafast dynamics in graphene of various doping, and can also provide new opportunities for graphene-based optoelectronic devices and applications.<sup>2–5</sup>

**Result and Discussion.** In this study, we employed the ion-gel gating technique because of its large tuning range and

**Received:** October 3, 2018

**Revised:** November 8, 2018

**Published:** November 19, 2018

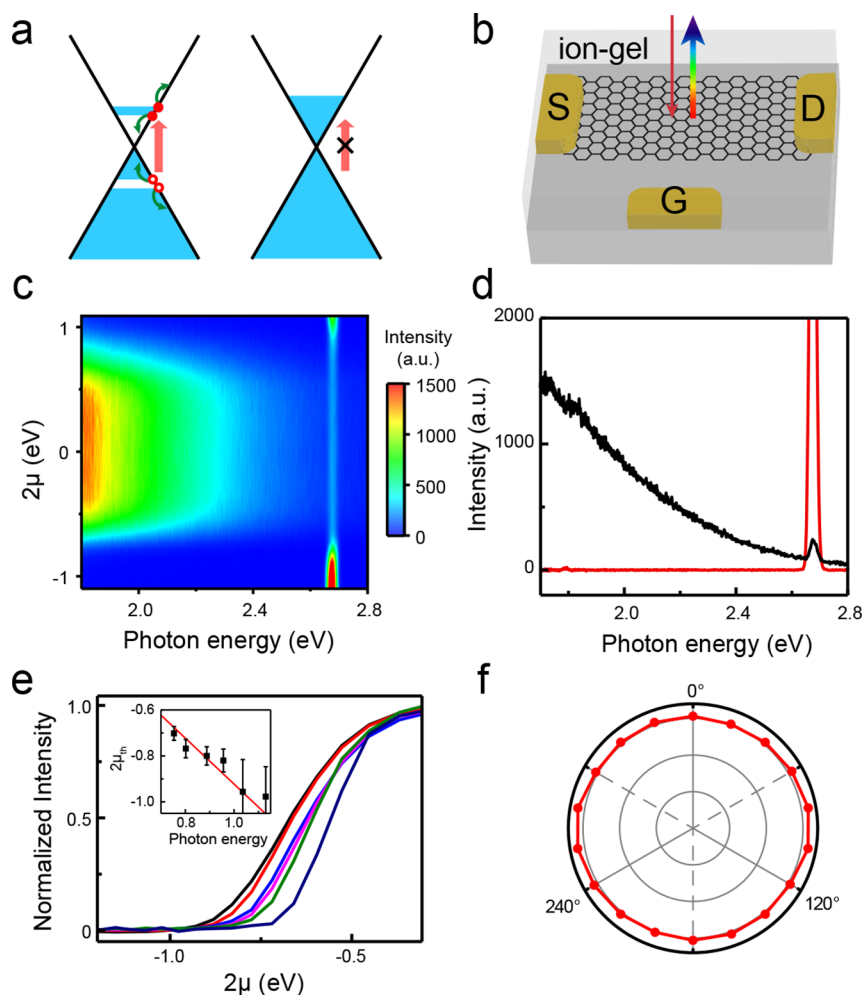


**Figure 1.** Gate tuning of ultrafast photoluminescence in ion-gel gated graphene. (a) Scenarios of optical excitation in undoped and doped graphene, respectively. With the tuning of chemical potential  $\mu$ , one-photon interband transition could be Pauli-blocked, thus affecting the ultrafast photoluminescence upon femtosecond excitation. (b) Schematic of ion-gel-gated graphene devices. Monolayer graphene was placed on fused silica substrate, while it was covered by ion-gel on the top. S, source electrode; D, drain electrode; G, gate electrode. (c) Photoluminescence spectra from ion-gel gated graphene as a function of chemical potential  $\mu$ . The excitation wavelength and incident fluence were 1400 nm (0.89 eV) and  $3.7 \text{ J/m}^2$ . The sharp peak at 2.67 eV corresponds to the third harmonic generation signal. All the optical spectra are corrected by the response curve of our detection system. (d) Photoluminescence spectra with chemical potential  $\mu$  at the CNP (black) and  $-0.89 \text{ eV}$  (red), respectively. (e) Photoluminescence intensity against chemical potential  $\mu$ . From the left to the right, the excitation photon energy was 1.13 eV (black), 1.034 eV (red), 0.956 eV (blue), 0.888 eV (magenta), 0.794 eV (green), and 0.753 eV (navy). The photoluminescence intensity was integrated from 1.828 eV (680 nm) to 1.883 eV (660 nm). Inset: the switch-off threshold  $2\mu_{\text{th}}$  as a function of excitation photon energy. The  $2\mu_{\text{th}}$  is determined by the chemical potential corresponding to 5% of the maximum photoluminescence intensity. To guide the eye, a red solid line with a slope of  $-1$  is plotted. (f) Azimuthal polarization pattern of the ultrafast photoluminescence.

optical transparency. With ion-gel as the dielectric material, the chemical potential,  $\mu$ , of monolayer graphene can be tuned up to 0.9 eV with respect to Dirac point.<sup>7,12</sup> Figure 1b shows the schematic of the ion-gel gated monolayer graphene device (see Methods for device fabrication). As in our previous work,<sup>12</sup> the chemical potential  $\mu$  as a function of gate voltages ( $V_g$ ) for our ion-gel graphene devices was determined through infrared transmission spectra (Figure S1), and the charge neutral point (CNP, for  $\mu = 0$ ) was identified from the peak position of source-drain resistance in transport measurement.

Figure 1c shows a 2D mapping of the photoluminescence spectra as a function of chemical potential  $\mu$ , when graphene was irradiated by femtosecond laser pulses with the photon energy of 0.89 eV (see Methods for experimental details). The photoluminescence signal remained almost unchanged when  $\mu$  varied near the CNP. But when  $\mu$  was further away from the

CNP, the luminescence intensity drastically dropped and was eventually quenched at high doping. This is very different from another nonlinear optical response we observed simultaneously, that is, the third harmonic generation (THG) signal at 2.67 eV, which became stronger at the higher doping level.<sup>12</sup> Two representative photoluminescence spectra are displayed in Figure 1d. Near CNP, the upconverted photoluminescence spectrum is very broad, which extends and gradually diminishes toward about three times of the incident photon energy.<sup>17–19</sup> At high doping level ( $\mu = -0.6 \text{ eV}$ ), no photoluminescence could be observed, suggesting its high on/off switching ratio by ion-gel gating.

For clarity, we plot the chemical potential dependence of the integrated photoluminescence intensity between 1.828 eV (680 nm) and 1.883 eV (660 nm) in Figure 1e. Different colors represent different excitation photon energies ( $\hbar\omega_0$ ),

ranging from 1.13 eV (black) to 0.753 eV (navy). In all cases, the luminescence intensity drastically drops near the one-photon transition ( $2\mu = \hbar\omega_0$ ). The greater the  $\hbar\omega_0$  was, the heavier doping is needed to switch off the photoluminescence. We defined the switch-off threshold to be 5% of the maximum photoluminescence intensity and plotted the corresponding  $2\mu_{\text{th}}$  versus  $\hbar\omega_0$  in the inset, which follows a straight line with the slope being  $-1$ . This further confirms that this ultrafast nonlinear photoluminescence originates from the one-photon resonant excitation in graphene as sketched in Figure 1a and ruled out the multiphoton excitation mechanism.<sup>6,12,17</sup>

We now discuss the emission process for this ultrafast upconverted photoluminescence with the focus on its  $\mu$ -dependence. As proposed previously for undoped graphene,<sup>17–19</sup> this photoluminescence results from the rapid Coulomb scattering in reduced dimension between photoexcited carriers, through which some carriers can gain energy from the others. Because of the electron–hole symmetry in undoped graphene, radiative recombination of those scattered electrons and holes can lead to this broadband, upconverted photoluminescence. Resulted from scattering, the luminescence loses information about the original incident dipole moment, and shows an isotropic polarization pattern (Figure 1f). When the chemical potential shifts away from CNP, the symmetry between electron and hole distributions is broken. To see its effect on the photoluminescence, we follow the previous work by Lui et al.,<sup>18</sup> which described this photoluminescence by the blackbody radiation from quasi-equilibrated hot carriers, characterized by an average temperature ( $\bar{T}_e$ ) through the relaxation process. Figure 2a shows the fitting of photoluminescence spectra at different chemical potential  $\mu$  using the Planck's law (see Supporting Information for details), from which we extracted  $\bar{T}_e$  versus  $2\mu$ , as shown in Figure 2b. When the chemical potential is near CNP,  $\bar{T}_e$  could reach more than 2500 K, consistent with previous studies. However, when the chemical potential  $|\mu|$  approaches  $\hbar\omega_0/2$ , the one-photon interband transition is nearly Pauli-blocked, both the luminescence and  $\bar{T}_e$  drop abruptly.

We can extract more information about the hot electron dynamics through the power dependence of the ultrafast photoluminescence, which varies with both  $\mu$  and the emission wavelength. Experimentally, at each given  $\mu$  we recorded the luminescence spectra at different laser excitation powers. One such example is shown in Figure S2 at  $\mu = 0$ . Meanwhile, at each emission wavelength we integrated the signal intensity within  $\pm 20$  nm around and plotted it against the excitation power. By fitting such plots with the power law, we obtained a mapping of the power index versus  $\mu$  and emission photon energy as shown in Figure 3a. Here the signal grows quadratically with the excitation power when the power index equals 2 and cubically when the power index is 3 and so on. The mapping exhibits two main features: (1) at a given emission wavelength, the power index increases rapidly with the chemical potential upon the one-photon resonance; (2) for a given chemical potential, emission at the shorter wavelength has the higher power index. These features are manifested in Figure 3b,c, showing two line-cuts along a constant  $\mu$  and a constant emission wavelength, respectively.

Physically, the power index reflects the times of upconverting scatterings experienced by hot carriers before the emission. Figure 3d displays four different scattering channels for electron–hole pairs leading to the upconverted luminescence at  $\mu = 0$ . Here we consider only the Auger-like, upconverting

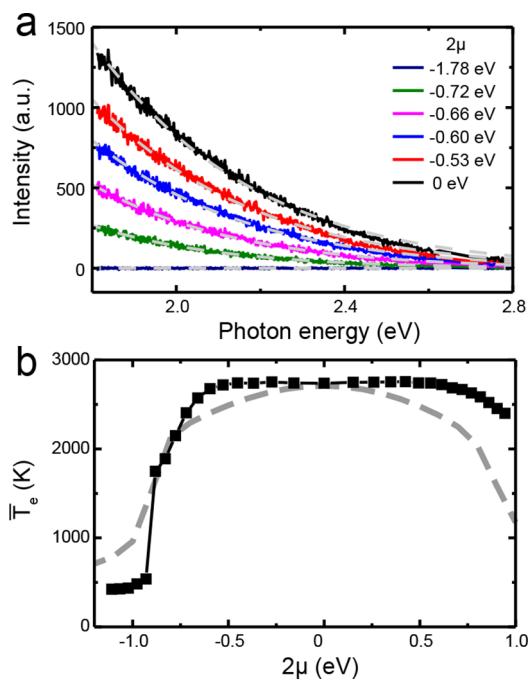


**Figure 2.** Temperature of hot carriers in gated graphene. (a) Ultrafast photoluminescence spectra at different chemical potentials with  $2\mu$  at CNP (black),  $-0.53$  eV (red),  $-0.60$  eV (blue),  $-0.66$  eV (magenta),  $-0.72$  eV (green), and  $-1.78$  eV (navy). Each spectrum was fitted to the blackbody radiation at different average carrier temperature ( $\bar{T}_e$ ), shown as the dashed lines. All the spectra shown above were taken from Figure 1c, and the third harmonic generation signal was subtracted. (b) The fitted  $\bar{T}_e$  of hot carriers as a function of  $2\mu$ . The gray dashed line is a theoretical curve derived from the model described in the text.

processes instead of the impact ionization.<sup>22–24</sup> These channels include: (1) e–e and h–h scatterings, through which an electron is scattered to higher energy by another electron, and a hole to a lower energy by another hole; (2) e–h and h–e scatterings; (3) e–e and e–h scatterings; (4) h–e and h–h scatterings. When such a scattering, e.g., the e–e and h–h channel, occurs for the first time, the highest possible energy gained by the upconverted electron–hole pair is  $\hbar\omega_0$ . The radiative recombination of this pair leads to the emission up to  $2\hbar\omega_0$ , and the scattering rate is proportional to the square of the hot electron/hole densities, yielding a power index close to 2. Experimentally, the emission photon energy could well exceed  $2\hbar\omega_0$ , meaning the scatterings must occur more than once before the final recombination, and the corresponding power index must be greater than 2 (Figure 3b). When  $\mu$  is tuned away from the CNP, some of the scattering channels are blocked due to the reduced phase volume, indicated by dashed lines with red crosses in Figure 3e. Therefore, compared to the case at CNP, more scatterings are needed for upconverted carriers to emit at the same photon energy, which explains the power index to increase as seen in Figure 3c.

More quantitatively, here we provide a model for describing all above features of the photoluminescence. In addition to the carrier–carrier interaction previously considered,<sup>22–24</sup> we further take into account of the carrier–optical phonon interaction as well as the effect of varying chemical potential. Upon femtosecond laser irradiation, the photoexcited carriers quickly establish a quasi-thermal equilibrium on the time scale of  $\sim 10$  fs.<sup>22–27</sup> Then they cool down rapidly by dumping

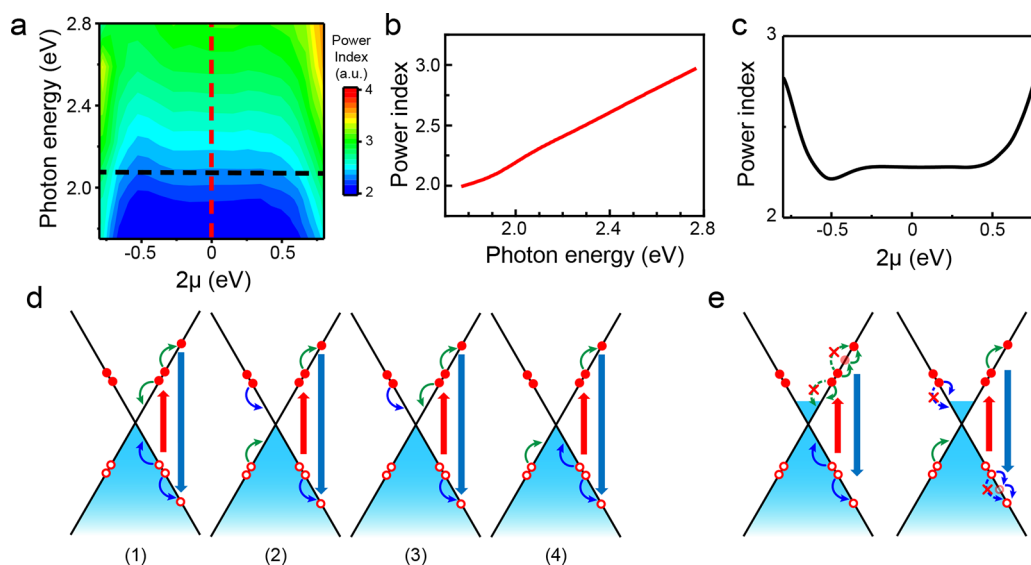


**Figure 3.** Analysis of power-dependent photoluminescence and the possible carrier–carrier scattering channels. (a) The 2D plot of power index at different chemical potential and emission photon energy. The power index was extracted from the power-dependent photoluminescence, as discussed in the text. The excitation wavelength was 1300 nm. (b,c) Line-cuts along the red and black dashed line in (a), respectively. (d) Four possible Auger-like scattering channels as discussed in the text. (e) Scenarios of reduced phase volume for scattering, when the chemical potential is tuned away from the CNP. The forbidden scattering processes are shown as dashed lines with red crosses.

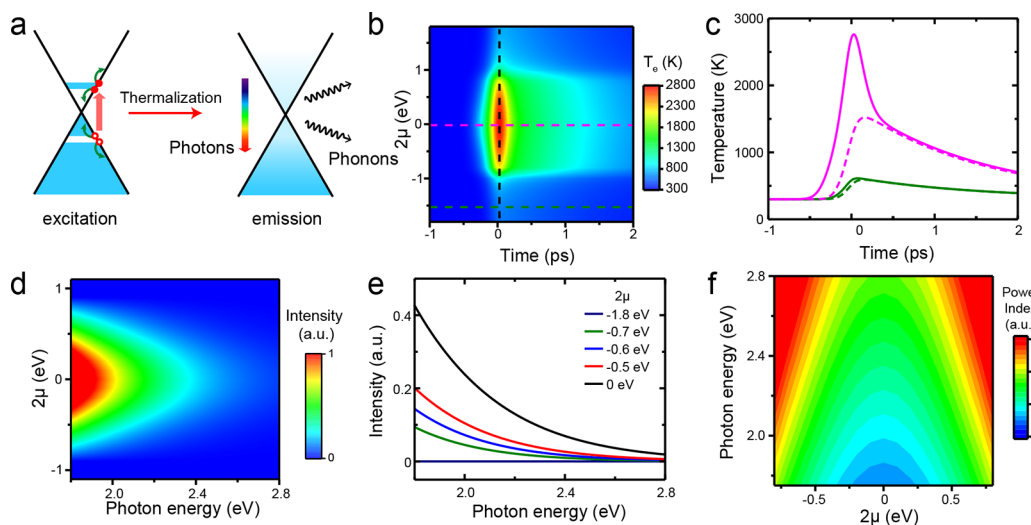


**Figure 4.** Theoretical simulation of the ultrafast photoluminescence. (a) Schematic illustrating the thermalization and relaxation processes of photoexcited carriers via carrier–carrier and carrier–phonon (optical phonons) interactions. Thus, the temperatures of carriers and optical phonons are separate, characterized by  $T_e$  and  $T_{op}$ . (b) Temporal evolution of carrier temperature  $T_e$  at different chemical potential. The simulation is conducted with 1400 nm, 200 fs, incident laser fluence of  $3.7 \text{ J/m}^2$ . (c) Temporal evolution of  $T_e$  (solid line) and  $T_{op}$  (dashed line) at different chemical potential  $\mu$ . The purple and green data correspond to  $\mu$  at CNP and  $-0.75 \text{ eV}$ , respectively. (d) The 2D plot of ultrafast photoluminescence, as calculated from the blackbody radiation of hot carriers. (e) Calculated photoluminescence spectra at different chemical potential. (f) Simulation of power index mapping at different chemical potential and emission photon energy.

energy to optical phonons within a few picoseconds (Figure 4a).<sup>22,23,28,29</sup> The entire process could be described by a two-temperature model, characterized by the instantaneous carrier temperature ( $T_e$ ) and optical phonon temperature ( $T_{op}$ ).<sup>18</sup> The temporal evolution of  $T_e$  and  $T_{op}$  could be solved numerically by considering the incident photon flux, the graphene absorption rate, the electron/optical phonon heat capacitance, and heat transfer rate between electrons and optical phonons (see Supporting Information for more details). Here both the absorption rate and carrier cooling rate are dependent on the chemical potential,<sup>20,21,30</sup> and we ignore the difference in electron and hole dynamics.<sup>31</sup>

Figure 4 shows the simulation results based on our two-temperature model with the excitation wavelength of 1400 nm, pulse duration of 200 fs, and absorbed fluence being  $8.5 \times 10^{-2} \text{ J/m}^2$  at CNP. As shown in Figure 4b,c, for undoped graphene ( $\mu = 0$ ),  $T_e$  rises to the peak value of 2800 K almost immediately following the excitation at time zero. Here the peak temperature is close to the average temperature we derived above, meaning that the majority of the photoluminescence occurs right after time zero.  $T_e$  then starts to drop as carriers dump energy to phonons, which is accompanied by the rise of  $T_{op}$ , until carriers and phonons reach a quasi-thermal equilibrium. When the chemical

potential is tuned away from the CNP, for example at  $\mu = -0.75$  eV,  $T_c$  is significantly lower than that at CNP for all the time. Again using the Planck's blackbody radiation law (see Supporting Information), we calculated the photoluminescence spectra in Figure 4d,e versus  $\mu$ . We could further simulate the behavior of power index, by varying the absorbed laser fluence at each emission photon energy and chemical potential (Figure 4f). All simulation results captured the essential features of our experimental data in Figure 1c and Figure 3a.

**Conclusion.** In summary, we reported the gate switching of ultrafast photoluminescence in monolayer graphene and analyzed its underlying mechanism both experimentally and theoretically. With the tuning of chemical potential in a wide range, the phenomenon can provide us with a deeper insight into the hot carrier dynamics in graphene. Our study may help the understanding of relevant processes in graphene such as carrier multiplication. Furthermore, this strong photoluminescence with its cutting-off behavior near the Fermi edge could be useful in many applications, such as sensing the local dielectric environment of graphene, and other graphene based optoelectronics and optical communication devices.<sup>32,33</sup>

**Methods. Device Fabrication.** Single crystalline or polycrystalline graphene monolayers used in the experiment were grown by CVD and transferred onto fused silica substrates. Source (S), drain (D) and gate electrodes (G) (50 nm Au and 5 nm Cr) were patterned through a dry stencil mask by electron beam deposition. All the electrodes were wire-bonded to a chip carrier for electrical control. Ion-gel gating was achieved by uniformly applying freshly prepared ion-gel solution onto the graphene devices and further drying in a glovebox filled with high purity argon gas. The ion-gel solution was prepared by dissolving 16.7 mg of poly(styrene-*b*-ethylene oxide-*b*-styrene) (PS-PEO-PS) and 0.5 g of 1-ethyl-3-methylimidazolium bis(trifluoromethylsulfonyl)imide ([EMIM][TFSI]) into 1.82 mL of dry dichloromethane.

**Characterization and Measurement.** The device characterization and experimental measurement were conducted in sample scanning optical microscopes that combined with femtosecond laser systems and an electrical transport setup. During the whole measurement, the graphene device was maintained in a dry nitrogen environment at room temperature. The charge neutral point of graphene was determined by its maximum resistance in response to the gate voltage. A Fourier transform infrared spectrometer (VERTEX 70) was used to measure the transmittance spectra of gated graphene from which the chemical potential at each gate voltage were deduced. For ultrafast photoluminescence measurements, a linearly polarized femtosecond laser beam tunable from 345 to 2500 nm at the repetition rate of 80 MHz was focused and normally incident on graphene through a microscopic objective (100 $\times$ , NA 0.95), and the reflected photoluminescence signal was collected. The sample sitting on a nano-positioning stage enabled us to locate defect-free areas on the sample. A fiber-coupled spectrograph equipped with a liquid nitrogen cooled silicon charge-coupled device was used to detect the photoluminescence after proper filtering.

## ■ ASSOCIATED CONTENT

### Supporting Information

The Supporting Information is available free of charge on the ACS Publications website at DOI: 10.1021/acs.nanolett.8b03967.

Additional information includes the details about extraction of hot carrier temperature from photoluminescence spectrum, power dependence of photoluminescence spectra, and theoretical simulation of hot carrier temperature and photoluminescence spectra (PDF)

## ■ AUTHOR INFORMATION

### Corresponding Authors

\*E-mail: wtliu@fudan.edu.cn.

\*E-mail: swwu@fudan.edu.cn.

### ORCID

Kaihui Liu: 0000-0002-8781-2495

Changgan Zeng: 0000-0001-8630-845X

Wei-Tao Liu: 0000-0003-0566-671X

Shiwei Wu: 0000-0001-9838-9066

### Author Contributions

D.H. and T.J. equally contributed to this work. S.W. and W.L. conceived and supervised the project. D.H., T.J., Y.Z., and Y.S. prepared the devices and performed the experiments with assistance from Y.D., L.S., and J.Z. on gate-dependent optical transmittance measurement. X.F., Z.Z., K.L., and C.Z. provided the CVD-grown graphene samples. D.H., T.J., W.L., and S.W. analyzed the data and wrote the paper with contributions from all authors.

### Notes

The authors declare no competing financial interest.

## ■ ACKNOWLEDGMENTS

We acknowledge Prof. Yuen-Ron Shen and Sheng Meng for insightful discussion. The work at Fudan University was supported by the National Basic Research Program of China (Grants 2014CB921601, 2016YFA0301002, 2016YFA0300900), National Natural Science Foundation of China (Grants 91421108, 11622429, 11374065), and the Science and Technology Commission of Shanghai Municipality (Grant 16JC1400401). K.L. was supported by Beijing Graphene Innovation Program (Z161100002116028). Part of the sample fabrication was performed at Fudan Nanofabrication Laboratory.

## ■ REFERENCES

- (1) Novoselov, K. S.; Geim, A. K.; Morozov, S. V.; Jiang, D.; Zhang, Y.; Dubonos, S. V.; Grigorieva, I. V.; Firsov, A. A. Electric field effect in atomically thin carbon films. *Science* **2004**, *306*, 666–669.
- (2) Bonaccorso, F.; Sun, Z.; Hasan, T.; Ferrari, A. C. Graphene photonics and optoelectronics. *Nat. Photonics* **2010**, *4*, 611–622.
- (3) Novoselov, K. S.; Fal'ko, V. I.; Colombo, L.; Gellert, P. R.; Schwab, M. G.; Kim, K. A roadmap for graphene. *Nature* **2012**, *490*, 192–200.
- (4) Koppens, F. H. L.; Mueller, T.; Avouris, P.; Ferrari, A. C.; Vitiello, M. S.; Polini, M. Photodetectors based on graphene, other two-dimensional materials and hybrid systems. *Nat. Nanotechnol.* **2014**, *9*, 780–793.
- (5) Xia, F.; Wang, H.; Xiao, D.; Dubey, M.; Ramasubramanian, A. Two-dimensional material nanophotonics. *Nat. Photonics* **2014**, *8*, 899–907.
- (6) Wang, F.; Zhang, Y.; Tian, C.; Girit, C.; Zettl, A.; Crommie, M.; Shen, Y. R. Gate-Variable Optical Transitions in Graphene. *Science* **2008**, *320*, 206–209.
- (7) Chen, C.; Park, C.; Boudouris, B. W.; Horng, J.; Geng, B.; Girit, C.; Zettl, A.; Crommie, M. F.; Segalman, R. A.; Louie, S. G.; Wang, F.

Controlling inelastic light scattering quantum pathways in graphene. *Nature* **2011**, *471*, 617–620.

(8) Mak, K. F.; He, K.; Lee, C.; Lee, G. H.; Hone, J.; Heinz, T. F.; Shan, J. Tightly bound trions in monolayer MoS<sub>2</sub>. *Nat. Mater.* **2013**, *12*, 207–211.

(9) Ross, J. S.; Wu, S.; Yu, H.; Ghimire, N. J.; Jones, A. M.; Aivazian, G.; Yan, J.; Mandrus, D. G.; Xiao, D.; Yao, W.; Xu, X. Electrical control of neutral and charged excitons in a monolayer semiconductor. *Nat. Commun.* **2013**, *4*, 1474.

(10) Ross, J. S.; Klement, P.; Jones, A. M.; Ghimire, N. J.; Yan, J.; Mandrus, D. G.; Taniguchi, T.; Watanabe, K.; Kitamura, K.; Yao, W.; Cobden, D. H.; Xu, X. Electrically tunable excitonic light-emitting diodes based on monolayer WSe<sub>2</sub> p–n junctions. *Nat. Nanotechnol.* **2014**, *9*, 268–72.

(11) Seyler, K. L.; Schaibley, J. R.; Gong, P.; Rivera, P.; Jones, A. M.; Wu, S.; Yan, J.; Mandrus, D. G.; Yao, W.; Xu, X. Electrical control of second-harmonic generation in a WSe<sub>2</sub> monolayer transistor. *Nat. Nanotechnol.* **2015**, *10*, 407–411.

(12) Jiang, T.; Huang, D.; Cheng, J.; Fan, X.; Zhang, Z.; Shan, Y.; Yi, Y.; Dai, Y.; Shi, L.; Liu, K.; Zeng, C.; Zi, J.; Sipe, J. E.; Shen, Y. R.; Liu, W.; Wu, S. Gate-tunable third-order nonlinear optical response of massless Dirac fermions in graphene. *Nat. Photonics* **2018**, *12*, 430–436.

(13) Tielrooij, K. J.; Orona, L.; Ferrier, A.; Badioli, M.; Navickaite, G.; Coop, S.; Nanot, S.; Kalinic, B.; Cesca, T.; Gaudreau, L.; Ma, Q.; Centeno, A.; Pesquera, A.; Zurutuza, A.; de Riedmatten, H.; Goldner, P.; García De Abajo, F. J.; Jarillo-Herrero, P.; Koppens, F. H. L. Electrical control of optical emitter relaxation pathways enabled by graphene. *Nat. Phys.* **2015**, *11*, 281–287.

(14) Mak, K. F.; Xiao, D.; Shan, J. Light–valley interactions in 2D semiconductors. *Nat. Photonics* **2018**, *12*, 451–460.

(15) Rivera, P.; Yu, H.; Seyler, K. L.; Wilson, N. P.; Yao, W.; Xu, X. Interlayer valley excitons in heterobilayers of transition metal dichalcogenides. *Nat. Nanotechnol.* **2018**, *13*, 1004.

(16) Mak, K. F.; Ju, L.; Wang, F.; Heinz, T. F. Optical spectroscopy of graphene: From the far infrared to the ultraviolet. *Solid State Commun.* **2012**, *152*, 1341–1349.

(17) Liu, W.; Wu, S. W.; Schuck, P. J.; Salmeron, M.; Shen, Y. R.; Wang, F. Nonlinear broadband photoluminescence of graphene induced by femtosecond laser irradiation. *Phys. Rev. B: Condens. Matter Mater. Phys.* **2010**, *82*, 081408.

(18) Lui, C. H.; Mak, K. F.; Shan, J.; Heinz, T. F. Ultrafast Photoluminescence from Graphene. *Phys. Rev. Lett.* **2010**, *105*, 127404.

(19) Stoehr, R. J.; Kolesov, R.; Pflaum, J.; Wrachtrup, J. Fluorescence of laser-created electron-hole plasma in graphene. *Phys. Rev. B: Condens. Matter Mater. Phys.* **2010**, *82*, 121408.

(20) Bistrizter, R.; MacDonald, A. H. Electronic Cooling in Graphene. *Phys. Rev. Lett.* **2009**, *102*, 206410.

(21) Viljas, J. K.; Heikkilä, T. T. Electron-phonon heat transfer in monolayer and bilayer graphene. *Phys. Rev. B: Condens. Matter Mater. Phys.* **2010**, *81*, 245404.

(22) Brida, D.; Tomadin, A.; Manzoni, C.; Kim, Y. J.; Lombardo, A.; Milana, S.; Nair, R. R.; Novoselov, K. S.; Ferrari, A. C.; Cerullo, G.; Polini, M. Ultrafast collinear scattering and carrier multiplication in graphene. *Nat. Commun.* **2013**, *4*, 1987.

(23) Gierz, I.; Petersen, J. C.; Mitrano, M.; Cacho, C.; Turcu, I. C. E.; Springate, E.; Stöhr, A.; Köhler, A.; Starke, U.; Cavalleri, A. Snapshots of non-equilibrium Dirac carrier distributions in graphene. *Nat. Mater.* **2013**, *12*, 1119–1124.

(24) Johannsen, J. C.; Ulstrup, S.; Cilento, F.; Crepaldi, A.; Zacchigna, M.; Cacho, C.; Turcu, I. C. E.; Springate, E.; Fromm, F.; Raidel, C.; Seyller, T.; Parmigiani, F.; Grioni, M.; Hofmann, P. Direct View of Hot Carrier Dynamics in Graphene. *Phys. Rev. Lett.* **2013**, *111*, 027403.

(25) Johannsen, J. C.; Ulstrup, S.; Crepaldi, A.; Cilento, F.; Zacchigna, M.; Miwa, J. A.; Cacho, C.; Chapman, R. T.; Springate, E.; Fromm, F.; Raidel, C.; Seyller, T.; King, P. D. C.; Parmigiani, F.;

Grioni, M.; Hofmann, P. Tunable Carrier Multiplication and Cooling in Graphene. *Nano Lett.* **2015**, *15*, 326–331.

(26) Shi, S. F.; Tang, T. T.; Zeng, B.; Ju, L.; Zhou, Q.; Zettl, A.; Wang, F. Controlling Graphene Ultrafast Hot Carrier Response from Metal-like to Semiconductor-like by Electrostatic Gating. *Nano Lett.* **2014**, *14*, 1578–1582.

(27) Song, J. C. W.; Levitov, L. S. Energy flows in graphene: hot carrier dynamics and cooling. *J. Phys.: Condens. Matter* **2015**, *27*, 164201.

(28) Winnerl, S.; Orlita, M.; Plochocka, P.; Kossacki, P.; Potemski, M.; Winzer, T.; Malic, E.; Knorr, A.; Sprinkle, M.; Berger, C.; de Heer, W. A.; Schneider, H.; Helm, M. Carrier relaxation in epitaxial graphene photoexcited near the Dirac point. *Phys. Rev. Lett.* **2011**, *107*, 237401.

(29) Wu, S.; Liu, W.; Liang, X.; Schuck, P. J.; Wang, F.; Shen, Y. R.; Salmeron, M. Hot Phonon Dynamics in Graphene. *Nano Lett.* **2012**, *12*, 5495–5499.

(30) Hanson, G. Dyadic Green's functions and guided surface waves for a surface conductivity model of graphene. *J. Appl. Phys.* **2008**, *103*, 064302.

(31) Horng, J.; Chen, C.; Geng, B.; Girit, C.; Zhang, Y.; Hao, Z.; Bechtel, H. A.; Martin, M.; Zettl, A.; Crommie, M. F.; Shen, Y. R.; Wang, F. Drude conductivity of Dirac fermions in graphene. *Phys. Rev. B: Condens. Matter Mater. Phys.* **2011**, *83*, 165113.

(32) Kim, Y. D.; Gao, Y.; Shiue, R.; Wang, L.; Aslan, O. B.; Bae, M.; Kim, H.; Seo, D.; Choi, H.; Kim, S. H.; Nemilentsau, A.; Low, T.; Tan, C.; Efetov, D. K.; Taniguchi, T.; Watanabe, K.; Shepard, K. L.; Heinz, T. F.; Englund, D.; Hone, J. Ultrafast Graphene Light Emitters. *Nano Lett.* **2018**, *18*, 934–940.

(33) Miyoshi, Y.; Fukazawa, Y.; Amasaka, Y.; Reckmann, R.; Yokoi, T.; Ishida, K.; Kawahara, K.; Ago, H.; Maki, H. High-speed and on-chip graphene blackbody emitters for optical communications by remote heat transfer. *Nat. Commun.* **2018**, *9*, 1279.